

www.acsami.org Research Article

3D Biofabrication of a Cardiac Tissue Construct for Sustained Longevity and Function

Matthew Alonzo, [⊥] Raven El Khoury, [⊥] Naveen Nagiah, Vikram Thakur, Munmun Chattopadhyay, and Binata Joddar*



Cite This: ACS Appl. Mater. Interfaces 2022, 14, 21800–21813



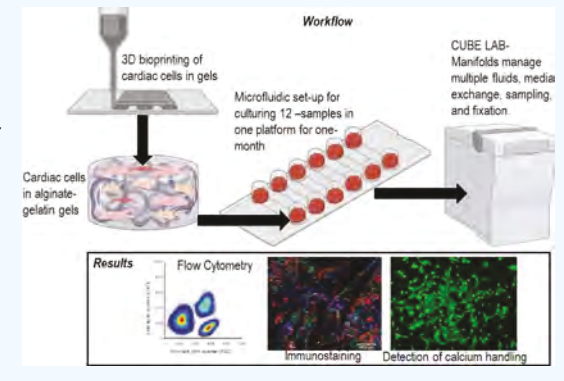
ACCESS

III Metrics & More

Article Recommendations

s Supporting Information

ABSTRACT: In this study, we developed three-dimensional (3D) printed annular ring-like scaffolds of hydrogel (gelatin—alginate) constructs encapsulated with a mixture of human cardiac AC16 cardiomyocytes (CMs), fibroblasts (CFs), and microvascular endothelial cells (ECs) as cardiac organoid models in preparation for investigating the role of microgravity in cardiovascular disease initiation and development. We studied the mechanical properties of the acellular scaffolds and confirmed their cell compatibility as well as heterocellular coupling for cardiac tissue engineering. Rheological analysis performed on the acellular scaffolds showed the scaffolds to be elastogenic with elastic modulus within the range of a native *in vivo* heart tissue. The microstructural and physicochemical properties of the scaffolds analyzed through scanning electron microscopy (SEM) and Fourier transform infrared spectroscopy-attenuated total



reflectance (ATR-FTIR) confirmed the mechanical and functional stability of the scaffolds for long-term use in *in vitro* cell culture studies. HL-1 cardiomyocytes bioprinted in these hydrogel scaffolds exhibited contractile functions over a sustained period of culture. Cell mixtures containing CMs, CFs, and ECs encapsulated within the 3D printed hydrogel scaffolds exhibited a significant increase in viability and proliferation over 21 days, as shown by flow cytometry analysis. Moreover, via the expression of specific cardiac biomarkers, cardiac-specific cell functionality was confirmed. Our study depicted the heterocellular cardiac cell interactions, which is extremely important for the maintenance of normal physiology of the cardiac wall *in vivo* and significantly increased over a period of 21 days in *in vitro*. This 3D bioprinted "cardiac organoid" model can be adopted to simulate cardiac environments in which cellular crosstalk in diseased pathologies like cardiac atrophy can be studied *in vitro* and can further be used for drug cytotoxicity screening or underlying disease mechanisms.

KEYWORDS: biofabrication, 3D bioprinting, cardiac tissue-on-a-chip, organoids, heterocellular coupling

1. INTRODUCTION

Engineering cardiac tissues in vitro involves recapitulating the three-dimensional (3D) extracellular matrix structures with relevant cardiac cells as seen in vivo. 1-5 Generation of cardiacspecific structures in vitro requires the integration of advanced technologies such as 3D biofabrication with a novel bioink mixed with cardiomyocytes, cardiac fibroblasts, and endothelial cells.⁶ The inclusion of cardiomyocytes in 3D biofabricated constructs is necessary for mimicking the similarity of such in vitro cardiac cell models to in vivo heart tissue. The addition of other cell types including cardiac fibroblasts and endothelial cells is an important strategy to improve the fidelity of the tissue-engineered myocardium. Cardiac fibroblasts secrete extracellular matrix and regulate this dynamic structure, in addition to providing mechanical support, electrical conduction, and paracrine signaling. 1-3,6,7 Endothelial cells are specifically included as they serve as the basic building block of vessel formation and paracrine signaling.

In previously published works, we developed cardiac tissue *in vitro* models with hydrogel scaffolds using 3D bioprinting with two dominant heterogeneous cell types, cardiomyocytes and cardiac fibroblasts that depicted cell coupling and heterocellular interaction.³ These engineered *in vitro* cardiac tissues exhibited cell proliferation, functionality, and sustained function.^{1–3} Based on such strong premise, in this study, we aimed to build upon the previously developed 3D cardiac organoid *in vitro* model with cardiomyocytes (CMs) and cardiac fibroblasts (CFs) by the inclusion of endothelial cells (ECs) within a unique bioink mixture for bioprinting of a platform that could exhibit sustained longevity and function-

Received: December 10, 2021 Accepted: April 25, 2022 Published: May 9, 2022





ality up to 21 days in culture. Normally, the generation of multiple cell-based tissue organoids suffers from tissue necrosis that occurs within the core of the 3D scaffolds. In this study, porous scaffolds with an optimized pore size and porosity were prepared by 3D bioprinting. The bioprinted scaffolds would permit the radial movement of media and nutrients from the lumen toward the periphery leading to the consistent increase in cell proliferation and function in all regions of the bioprinted structure. Furthermore, the equal distribution of culture medium, nutrients, and oxygen would promote the growth and maintenance of the tissue throughout the scaffold.

For maintenance of optimal cell function, relatively soft bioinks are preferred for printing, although these undergo significant deformation during the printing process, which may impair shape fidelity and long-term sustenance of the cell-gel printed 3D constructs. An alginate-gelatin-based bioink containing sodium alginate with high guluronic acid content that is known to exhibit superior viscosity and gelling properties desirable for an extrusion-based 3D printing operation was used.8 Inclusion of gelatin is known to be favorable as it presents the RGD sequence and enhances biocompatibility of scaffolds. Since the alginate polymer plays a major role in the gelling of the hydrogels, increasing the content of G residues in the chains is known to correlate positively with the gelling properties of alginate leading to more strong gels that can be maintained in culture for longer periods. 10 Especially, the G blocks also play an important part in the alginate gel network formation and stabilization.

Using such a bioink with advanced rheological and chemical cross-linking parameters is expected to yield 3D structures with higher shape fidelity and long-term maintenance. The resultant constructs can then be used to perform long-term studies such as the evaluation of the effects of acute and chronic environmental stressors and drug cytotoxicity on cardiac tissue functions.

It is hypothesized that a 3D bioprinted cardiac organoid system using three major cardiac cell types (CM, CF, and EC) in such a structurally robust and well-designed *in vitro* model will promote enhanced cell—cell signaling and accelerate cell growth and tissue maturation by allowing cells to self-organize and facilitate unrestricted interactions between other cells and their surroundings. It may be of added advantage to adopt 3D bioprinted organoid models, as the coupled cells will be entrapped within a gel-like scaffold preventing their untimely dissociation from a normal adherent culture system during *in vitro* culture.

This experiment was developed to be housed inside the CubeLab, an autonomous space station module designed by Space Tango based in Lexington, KY. The design produced from this work will be used to send the defined experiment to the ISS for 1 month after the completion of this study. The CubeLab and TangoLab systems are research frameworks, which allow for low-cost, microgravity-based research opportunities to be pursued under both Earth's gravity and microgravity conditions.

2. MATERIALS AND METHODS

2.1. Materials. Medium viscosity sodium alginate containing a higher guluronic acid (G-block content >60% as specified by the manufacturer) was obtained from Pronova UP MVG (Nova Matrix, FMC, Norway) and gelatin from porcine skin (~300 g Bloom; Sigma-Aldrich, St. Louis, MO), which were the main components of the bioink mixture. Ionic cross-linking solution for the hydrogel scaffolds

consisted of calcium chloride dihydrate (Fisher Chemical, Germany) mixed in phosphate-buffered saline (PBS) 1× solution (Fisher Bioreagents). Paraformaldehyde solution (PFA, 4% in PBS, Janssen Pharmaceuticals, Belgium) was applied for cell fixation within the bioprinted scaffolds.

2.1.1. Materials Used for Cell-Based Experiments. Cardiac fibroblast complete growth medium (Cat. No. 316500, Cell Applications Inc., CA) was used to culture human cardiac fibroblasts (HCF 306A-05a, Cell Applications Inc., CA). The AC16 human cardiomyocyte cell lines (SCC109, EMD Millipore, MA) were cultured and expanded in Dulbecco's modified Eagle's medium (DMEM/F12; Sigma Cat. No. D6434) containing 2 mM L-glutamine (EMD Millipore Cat. No. TMS-002-C), 12.5% FBS (EMD Millipore Cat. No. ES-009-B), and 1× penicillin-streptomycin solution (EMD Millipore Cat. No. TMS-AB2-C). Human cardiac microvascular endothelial cells (HCMECs; C12285; Millipore-Sigma) were grown in endothelial cell growth medium MV 2 basal medium with growth kit (C-22022; Millipore-Sigma) containing 0.05 mL of fetal calf serum, 5 ng of epidermal growth factor (recombinant human), 10 ng of basic fibroblast growth factor (recombinant human), 20 ng/mL of insulin-like growth factor (long R3 IGF), 0.5 ng/mL of vascular endothelial growth factor 165 (recombinant human), 1 µg/mL of ascorbic acid, and 0.2 μ g/mL of hydrocortisone combined as per the manufacturer's protocol. Combined growth media (as detailed in Section 2.5.1) was prepared by mixing the respective growth medium for CM, CF, and EC in a 2:2:1 volume ratio. This was done to reflect and mimic the ratios in which cells were mixed and printed within the 3D scaffolds in this study. For all contractile cell-scaffold experiments, the murine cardiomyocyte cell line HL-1 (SCC065; Millipore-Sigma) was used⁹ since the AC16 CM does not depict this behavior. HL-1 cells were cultured based on vendor's protocols using growth medium that consisted of Claycomb medium (51800C; Millipore-Sigma), supplemented with 100 μM norepinephrine, 10% fetal bovine serum (FBS), and 4 mM L-glutamine that helped maintain the HL-1 cell line and the mature cardiomyocyte behavior.

PKH67 Green Fluorescent Cell Linker Mini Kit, PKH26 Red Fluorescent Cell Linker Mini Kit (Sigma-Aldrich), CellTrace Violet, proliferation kit (Invitrogen, Carlsbad, CA), and DAPI (Thermo Fisher Scientific) were used as cell labeling dyes. In addition, 24- and 6-well flat-bottom plates (Thermo Fisher Scientific) were used for *in vitro* cultures. Trypsin—ethylenediaminetetraacetic acid (EDTA, 0.25%, phenol red, Thermo Fisher) was used for cell detachment.

2.2. Preparation of Bioink. To obtain an optimized composition of the bioink containing alginate and gelatin, we methodically added small amounts of MVG alginate and gelatin to make it extrudable under shear pressure. At least seven different compositions were attempted for extrusion printing containing a mixture of alginategelatin in the following (w/v) percentages, 4%-4%, 4%-2%, 4%-1%, 1%-4%, 2%-4%, 7%-10% and 7%-5%, along with a cross-linking solution of calcium chloride (CaCl₂) varying from 80 to 100 mM concentration, after which an optimized composition was established (see the Supporting Information section). The optimized solution was made using 10% (w/v) gelatin dissolved in PBS (pH 7.4) under light heat and constant mixing with a magnetic stirrer under sterile conditions. Another solution of 14% (w/v) sodium alginate was made with or without cell suspension (see Section 2.5.1) in combined growth media in a 5 mL conical tube. Both solutions were consolidated into a separate 5 mL concial tube so that the final concentration was 5% (w/v) gelatin and 7% (w/v) alginate. The mixture was allowed to dissolve overnight at room temperature and then centrifuged at 1200 rpm for 3 min to remove air bubbles. All gels were UV-sterilized for 15 min before loading into printing cartridges or mixing with cells.^{3,13} Based on prior published works from our laboratory, this is not known to affect the gels. For biological studies, the bioink was mixed with cells using the procedure detailed in Section 2.5.1 and loaded into a 3 mL syringe-printing cartridge with a 20 G tapered conical nozzle (CELLINK, Blacksburg, VA). Acellular gels were loaded without mixing of cells for material characterization studies.

2.3. Three-Dimensional (3D) Bioprinting. For all material characterization experiments using acellular scaffolds, 3D annular rings bioinspired from inherent structures of blood vessels and tissueengineered vascular grafts with a diameter of 5 mm and 1 mm in height were designed using SolidWorks software. For cell-based studies, and integration of the 3D bioprinted tissue chip within the hardware platform provided by Space Tango, a waffle-mesh-like design (12 mm × 12 mm × 1 mm) was adopted. All designs were converted to a binary.stl file using Meshmixer, a prototype designer tool. Using CELLINK BIO X (Blacksburg, VA), a pneumatic head was used to print structures directly within wells of a 12-well plate. The optimized bioprinting parameters are tabulated in Table 1. After

Table 1. Optimized Bioprinting Parameters

parameter	specification
nozzle diameter	Tapered 20 G
printing speed	2 mm/s
pressure	80 kPa
temperature	27 °C
infill	30%

3D structures were printed, they were cross-linked with 100 mM $CaCl_2$ by pipetting 500 μ L of the ionic solution into the wells and placed on a Belly Dancer Shaker (IBI SCIENTIFIC, Iowa) at 10 rpm. The solution was removed from the wells after 5 min. The structures were washed three times with sterile PBS prior to experimentation.

- 2.4. Material Characterization. Scaffolds were printed and cross-linked, after which they were analyzed to determine their material and physicochemical parameters as well as study their microstructure to correlate with cell behavior and function later in this study. All acellular gels were loaded with cell-free media for the material characterization studies.
- 2.4.1. Swelling and Degradation Analysis. Samples were subjected to swelling in 1 mL of combined growth media for 3, 10, and 21 days at 37 $^{\circ}$ C and 5% CO₂ (as in Section 2.5.1). The samples were imaged at the respective time points to detect and locate signs of macroscopic physical degradation of the 3D structures. During this 21 day experiment, culture media was changed every 5 days. Prior to swelling, the structures were maintained at -80 °C overnight and then lyophilized. The initial dry weights (W_0) of the lyophilized structures were recorded. After submerging the structures in media, their weights (W_t) at different time intervals after swelling were recorded. After all samples were evaluated, a swelling ratio (D_s) for each sample was calculated using the following equation

$$D_{\rm s} = W_{\rm t} - W_0 / W_0 \tag{1}$$

Scaffolds printed without cells were used in this experiment to assess the swelling and degradation behavior of the material present in the scaffolds irrespective of the cells.

2.4.2. Scanning Electron Microscopy. SEM micrographs were acquired from acellular printed scaffolds at varying time points in culture to study the effect of environmental degradation and culture on the scaffolds. The average pore diameter of the acellular crosslinked 3D printed scaffolds was measured at 3, 10, and 21 days in culture conditions by analyzing electron micrographs of crosssectioned lyophilized samples. The lyophilized samples were sputter-coated with gold/palladium (2-3 min) in a sputter coater (Gatan Model 682 Precision etching coating system, Pleasanton, CA) and visualized using SEM (S-4800, Hitachi, Japan) at 7 kV voltage and a current of $5~\mu A$ at varying magnifications. Collected images obtained were analyzed using Image J to determine the average pore diameter during each time point. A total of at least n = 5 images per sample were assessed for samples evaluated at varying time points.

2.4.3. Attenuated Total Reflectance Fourier Transform Infrared Spectroscopy (ATR-FTIR). Acellular scaffolds were used for ATR-FTIR absorbance, and measurements were carried out with the samples at 3 and 21 days in culture using a Nicolet FTIR spectrometer (Thermo Fisher Scientific) equipped with a diamond

ATR crystal. The spectrum of the samples was recorded from 400 to 4000 cm⁻¹ to assess the chemical stability of the scaffolds and varying degrees of degradation at different time points. An average of 32 scans per sample were averaged to reduce spectral noise.

2.4.4. Rheological Analysis. Scaffolds printed with and without cells were used in this experiment to assess the mechanical behavior of the material present in the scaffolds irrespective of the cells and in the presence of cells. For cell-based scaffolds, AC16 CM cells (Section 2.1.1) were mixed in the bioink to constitute a final cell seeding density of 1×10^6 cells/mL and printed to study the rheological properties of cell-based scaffolds in comparison with acellular controls. Rheometry analysis of the samples was conducted on an Anton-Paar MCR 92 rheometer (Anton-Paar, Austria) with a PP25/S measuring system and a 25 mm parallel plate with a 1 mm gap between the plate and the stage. The viscosity of non-cross-linked and cross-linked bioink samples was tested in a continuous flow experiment at room temperature to elucidate the effect of crosslinking on the printed constructs. The samples were assessed with a ramped shear rate from 0.1 to 100 Hz to determine if the material exhibited shear-thinning properties. To determine the limit of the material's linear viscoelastic range and yield stress, small amplitude oscillatory shear was applied to the samples in an amplitude sweep with a strain from 0.1 to 150% at a constant frequency of 1 Hz. From this evaluation, an optimal strain within the linear viscoelastic region was chosen to be kept constant during a frequency sweep from 100 to 0.1 rad/s. The mechanical properties of the cross-linked 3D printed hydrogel scaffolds were evaluated 3, 10, and 21 days after swelling in PBS. These cross-linked structures were allowed to swell in 6-well plates with PBS (pH 7.4). Storage/loss moduli, complex viscosity, and elastic modulus were measured at 1.99 Hz as previously done and reported^{3,13} to analyze the mechanical stability of the scaffolds at various times.

2.5. Biocompatibility Studies. For all cell-related experiments in this study, scaffolds with cells were printed and cross-linked, after which they were analyzed to determine cell behavior and function, and assessment of scaffold biocompatibility.

2.5.1. Cell Culture and Encapsulation. For evaluation of biocompatibility of the bioink, contractile HL-1 cells were mixed in the bioink to constitute a final cell seeding density of 1×10^6 cells/mL and printed to study their contractile behavior visually in bioprinted gels or on two-dimensional (2D) control wells. For this experiment, the HL-1 cells were cultured according to the manufacturer's protocol and stabilized for at least three passages prior to bioprinting. Cells printed within the alginate-gelatin gels consisting of a fibronectingelatin mixture at a 0.04 mg/mL concentration were rinsed with HEPES buffered Tyrode's solution (Thermo Fisher Cat. No. 50151910) followed by the addition of 1.5 mL per well of 5 μ M Fluo-8AM solution and incubated at 37 °C for 1 h. The purpose of using Fluo-8AM was to adopt a fluorescence-based assay for detecting intracellular calcium mobilization in these cells that can indirectly correlate with their contraction behavior and cardiac function. The gels with HL-1 cells were rinsed with Tyrode's solution and immediately observed under the fluorescent microscope (ZEISS LSM, Germany) with an FITC filter. To assess the long-term effects of the 3D bioprinted gels on the HL-1 cells, cells were manually detached and trypsinized from the gels and counted at varying time points using a hemocytometer to study their proliferation within the 3D environments as well as confirm their overall biocompatibility up to a 21 day culture period.

For bioprinting of the cardiac organoids, CMs (AC16), CFs (HCF), and ECs (HCMEC) were mixed in a ratio of 2:2:1 based on guidance derived from published studies to constitute a final cell seeding density of 2×10^6 cells/mL (800,000 CM: 800,000 CF: 400,000 EC). ^{14,15} All cells were grown, stabilized, and prestained with PKH26 (red for CM), PKH67 (green for CF), and Cell Tracker Violet (blue for EC) according to the manufacturer's protocol. Stained cells were pooled into one pellet for bioprinting. This cell pellet was resuspended in 75–90 μ L of PBS and added to the bioink mixture into the 5 mL conical tube containing 2 mL of bioink. The cells were mechanically mixed with the hydrogel and loaded into a

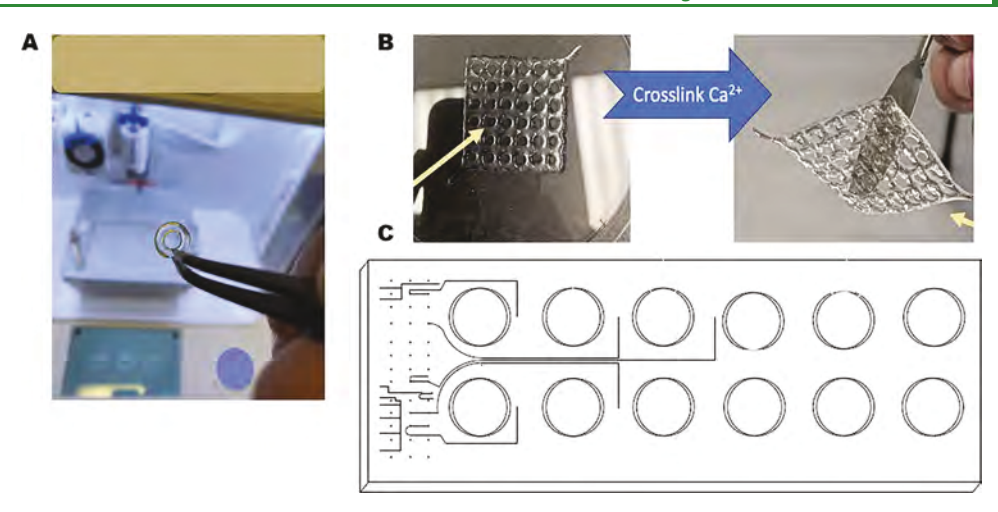


Figure 1. 3D printed cardiac scaffolds were developed, and their properties were studied up to 21 days. (A) Rigid 3D printed structures developed through optimized printing parameters. (B) High-throughput 12-well fabrication of the 3D printed scaffolds and their integration within the CubeLab microfluidic channel-based system. (C) A schematic of the high-throughput assembly of the bioprinted scaffolds in 12-well plates and the workflow.

sterile 3 mL syringe using a female luer connector (Cat. No.06-713-070, Fisher Scientific) and 3D bioprinted using optimized parameters, as summarized in Table 1. After bioprinting, cardiac organoids were maintained in 1 mL of media in each well of a 24-well plate for longterm culture using the combined media, composed of the respective media used for each cell type (CM-CF-EC) mixed in the same ratio

2.5.2. MTS (3-(4, 5-Dimethylthiazol-2-yl)-5-(3-carboxymethoxyphenyl)-2-(4-sulfophenyl)-2H-tetrazolium) Assay. To assess the viability of the encapsulated cells in the hydrogel, at various time points, the culture medium was removed and a tetrazolium salt, MTS, was added in the ratio of 1:10 (MTS solution: media). After incubation of the MTS reagent with the samples for 4 h at 37 °C, the absorbance of each well was measured at 490 nm.

2.5.3. Heterocellular Coupling. The interaction between the cells encapsulated in the hydrogels was evaluated by assessing the total number of heterocellular couplings between cells. Cell-laden 3D bioprinted hydrogel scaffolds were immersed in 4% paraformaldehyde solution for 15 min at room temperature (25–28 °C) to fix cells prior to confocal fluorescent microscopy imaging (Nikon Eclipse NiE). The CMs were stained using PKH26 (red), the CFs were stained using PKH67 (green), and the ECs were stained using Cell Tracker Violet (blue). The average coupling percentage was obtained using eq 2. At least three stacked images were utilized for calculating the average percentage of heterocellular coupling. In any image chosen for the analysis, the number of adjacent CMs, CFs, or ECs coupled was counted within a 100 by 100 μ m area for the calculation of percentage (%) cell coupling in this study. To satisfy this requirement, at least two types of cell coupling between CM, CF, and EC were identified and accounted for the % reported

% coupling =
$$\frac{\text{# of CMs (red), CFs (green) and EC (blue)}}{\text{total no. of cells in the selected image}}$$
× 100 (2)

2.5.4. Flow Cytometry (FACS) Analysis. Cardiomyocytes were prestained using the CellTrace Violet (CTV) Cell Proliferation Kit (Invitrogen, Carlsbad, CA) according to the manufacturer's protocol prior to 3D bioprinting with the cardiac fibroblasts in alginate-gelatin hydrogel. Similarly, cardiac fibroblasts were stained with the CellTrace Yellow (CTY) Cell Proliferation Kit and the endothelial cells were stained with the CellTrace Far Red (CTFR) Cell Proliferation Kit for FACS analysis. The 3D scaffolds with cells were cut using a blade, and cells were extracted using a Miltenyi gentleMACS Dissociator (Miltenyi Biotec, Cambridge, MA) using a Multi Tissue Dissociation Kit-1 by running the Multi_B program according to the

manufacturer's protocol. After 3, 10, and 21 days, the extracted cells from scaffolds were fixed with 4% PFA for 15 min at room temperature and added to their designated FACS analysis falcon tubes and analyzed using a Beckman Coulter Gallios Flow Cytometer (Brea, CA) using the following excitation and emission wavelengths of 405 and 450 nm for CTV, excitation at 546 nm and emission at 579 nm for CTY, and excitation at 630 nm and emission at 661 nm for CTFR, respectively.

Positive controls included freshly isolated and prestained cells using the above-mentioned dyes for each cell type that were analyzed using FACS, respectively. On the contrary, negative controls included freshly isolated and nonstained cells that were analyzed using FACS.

2.5.5. Immunostaining. Immunohistochemical analysis was performed to detect connexion-43 (CX43) and myosin heavy chain (MyoH) in the HL-1 cells, whereas the expression of PECAM-1 was probed in the EC cells used in this study. In addition, to confirm the heterocellular coupling among the CM and CF cells, they were probed using the fibroblast-specific protein 1 (FSP-1) for CF and the AC16 CMs were labeled with CX43 when the cells were cocultured in vitro. Prior to the addition of EC to the CM-CF-containing gels, we confirmed the heterocellular coupling between CM and CF that has been established by prior studies in our laboratory.^{3,13}

The HL-1 cells in 3D gels were rinsed in 1× phosphate-buffered saline (PBS) and subsequently fixed in methanol for 15 min. The cells were then blocked for 1 h at room temperature, washed once, and incubated with either of the primary antibodies CX43 (1:400, Cell Signaling, Danvers, MA; or 1:300, Thermo Fisher Scientific, Waltham, MA) overnight at 4 °C. The cells were then washed three times and probed with secondary antibodies, Alexa Fluor 594 goat antirabbit IgG and Alexa Fluor 488 goat antimouse IgG (1:2000; Thermo Fisher Scientific, Waltham, MA), and incubated at room temperature for an hour. After 3 washes with 1× PBS, the cells were stained with Hoechst solution (1: 50,000) for 3 min and rinsed with 1× PBS, mounted on glass slides using Fluoromount G mounting media (Electron Microscopy Sciences, Fort Washington, PA). The images were acquired using a Nikon Eclipse Ni-E microscope (Nikon Instruments Inc., Melville, NY).

To confirm the colocalization of the printed EC and confirm their paracrine signaling for the maintenance of cardiac functionality within the printed constructs, the expression of PECAM-1 (also known as CD31) was probed. We expected PECAM-1 expression to be associated with intact endothelial cell intercellular junctions, where it functions as a mechanosensor and in the maintenance of junctional integrity. As described in Section 2.5.3, the cardiomyocytes and the cardiac fibroblasts were prestained using PKH-dyes to depict their heterocellular coupling,3 while the third cell type, endothelial cells,

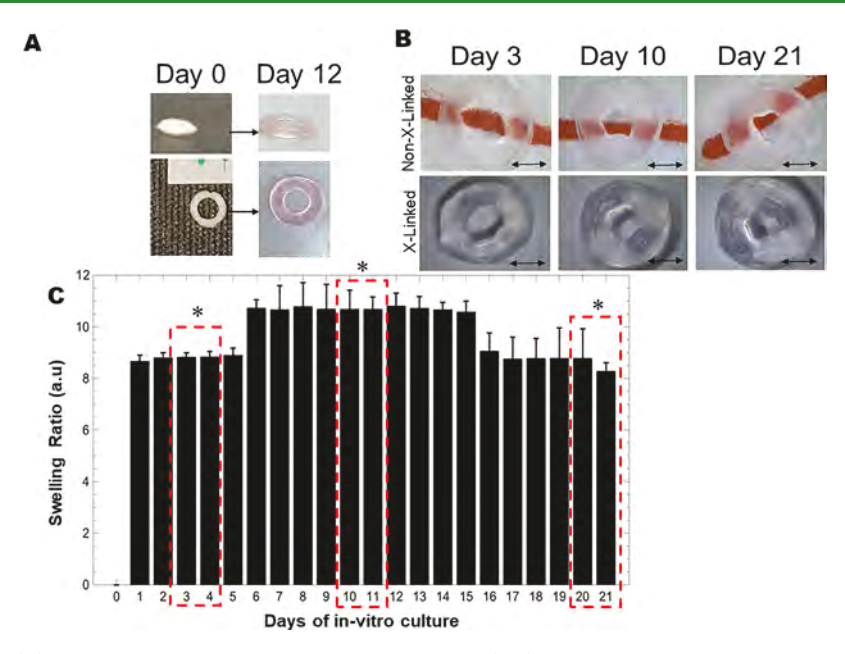


Figure 2. Swelling analysis. (A) Lyophilized 3D printed annular ring on day 0 (left) and swollen annular ring on day 12 (right). (B) Non-crosslinked versus cross-linked scaffolds shown during the swelling experiment at varying time points. Scale bar in all images corresponds to 2 mm. (C) Swelling ratio of the 3D printed annular rings at various time points in culture media with 3-4 days, 10-11 days, and 20-21 days highlighted to depict significant differences in swelling behavior in the scaffolds studied. Swelling ratio (mean ± SD) for characteristic alginate-gelatin-annular ring scaffolds was studied for 21 days during which the maximum degree of swelling was attained on day 12. Beyond day 12, until day 15, the swelling apparently reached equilibrium as these values did not seem to bear any statistical differences when analyzed and a significantly lower swelling ratio from day 16 to 21 was observed.

was not prestained for this experiment. At the end of the culture period, the cell-gel scaffold was collected, fixed with 4% paraformaldehyde for 15 min, washed with PBS 3 times, and incubated with a blocking solution (PBS with 1% NGS and 0.3% Triton X-100) for 60 min. The samples were washed once and incubated with the primary antibody anti-CD31 (1:400; Cell Signaling, Danvers, MA) overnight at 4 °C followed by three washes. Alexa Fluor 350 goat antirabbit IgG (1:2000; Thermo Fisher Scientific, Waltham, MA) was added as a secondary antibody and incubated for 1 h at room temperature. Slides were treated to three washes and mounted in Fluoromount G (Electron Microscopy Sciences, Fort Washington, PA). CD31 stained samples were imaged (Nikon Instruments Inc., Melville, NY) for detection and colocalization of the EC along with two other cardiac cell types, namely, CM

2.6. Hardware Implementation for Sustained Culture. Hardware integration includes the physical incorporation of the 3D bioprinted cardiac tissue samples into the Space Tango 9U CubeLab infrastructure, with $1U \sim 10 \text{ cm}^3$ as the standard size, with in-built temperature and pH controls required by a variety of science and subsystems.¹⁶ All hardware is designed to fit with the form factor constraints of a Spaceflight half locker. Culture manifold and chip holders are designed by Space Tango in consultation with our team. Briefly, the manifold was made from polyether ether ketone (PEEK) and has 24 wells (2 × 12 wells) circulated with complete growth media at a rate of 0.5 mL/min, similar to other organ-on-chip-type experiments. Each well can accommodate a 3D printed cardiac tissue sample or a 2D control (on a glass coverslip) placed atop sample wells. A slow refreshment of fresh media at a rate of $\sim 10-20 \,\mu\text{L/s}$ up to 1 min will be used to supplement fresh media to the wells with the 3D and 2D samples for up to 21 days.

2.7. Statistical Analysis. All experiments were performed in triplicate, and values were expressed as mean ± standard deviation. All data were compared using a one-way ANOVA with a post hoc Tukey's multiple comparison test with p < 0.05 considered statistically significant.

3. RESULTS

3.1. Biofabrication. Figure 1A,B depicts the transparent and rigid 3D printed scaffolds made with the in-house prepared gelatin-alginate (5-7%) bioink along using parameters listed in Table 1. The ionic cross-linking of the sodium alginate in the hydrogel mixture with 100 mM of calcium chloride solution was found to be beneficial in obtaining structurally stable 3D printed hydrogels for sustained periods. It is expected that the bioink mixture containing gelatin and alginate would lead to physical chain entanglements between the two polymeric chains resulting in electrostatic interactions between the two proximal subunits.¹⁷ Figure 1C shows a schematic of the high-throughput assembly of the bioprinted scaffolds in 12-well plates and the workflow and integration of the 3D bioprinted cardiac tissue platform within the CubeLab platform provided by Space Tango signifying the consistency and reproducibility of the bioprinted structures.

3.2. Swelling Analysis. Structural fidelity and integrity of the 3D printed hydrogels were evaluated through swelling studies, which revealed that all structures sustained 3 weeks of in vitro culture, as shown in Figure 2A,B. Representative images of lyophilized and swollen scaffolds at equilibrium are shown in Figure 2A. As shown by our data, scaffolds attained maximum equilibrium swelling after 6 days of incubation and maintained this trend until 15 days (Figure 2C). A significant reduction in swelling was observed on day 16 signifying the onset of bulk degradation of the scaffold, as shown in Figure 2C. Overall, a high structural fidelity of the 3D bioprinted structures maintained throughout the study confirmed its macrostructural stability. The macrostructural stability also implied minimum to no microstructural degradation, which signifies the generation of an intricate scaffold with a large set of interconnected pores for media perfusion that can mimic

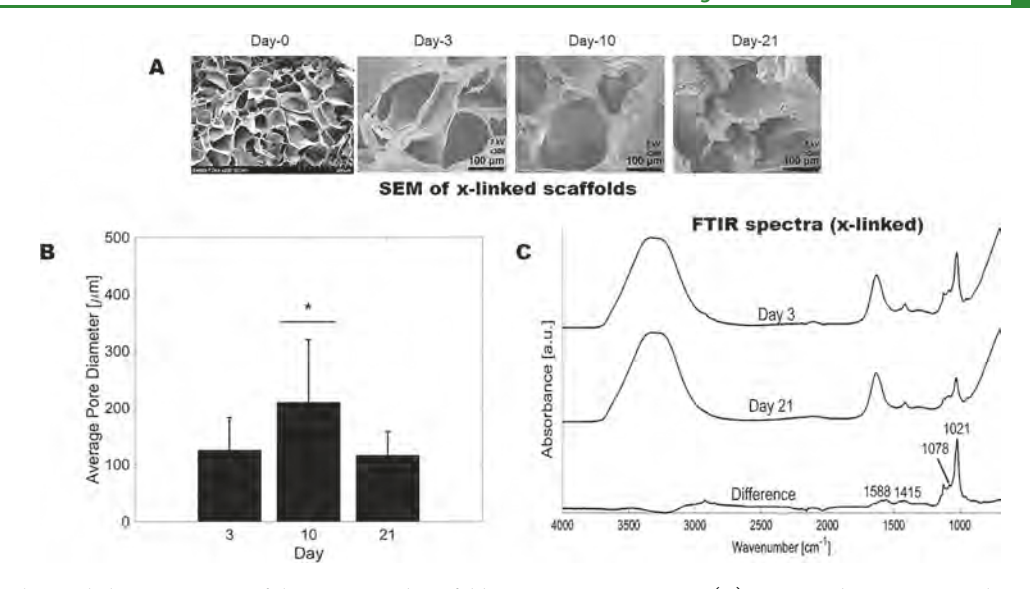


Figure 3. Physicochemical characterization of the 3D printed scaffolds at various time points. (A) Gross and microstructural analysis (using SEM) of the 3D printed annular ring scaffolds showing average pore diameters at various time points. (B) Average pore diameters of scaffolds at varying time points in the culture. (C) ATR-FTIR of the 3D printed scaffolds on days 3 and 21 showing minimal chemical degradation of the scaffolds.

natural microenvironments via several spatially organized cell niches found in the cardiac tissue for cell localization.

3.3. Microstructural Analysis and Characterization. Microstructural stability of the 3D scaffolds was evaluated using SEM images acquired on days 0, 3, 10, and 21, as shown in Figure 3A. The average pore diameter was assessed to be within a range of $117 \pm 41 - 126 \pm 57 \,\mu\text{m}$ at 3 and 21 days, respectively (Figure 3B). The significant increase in the pore diameter at the day 10 time point was due to the swelling of the structures, as indicated by our data presented earlier in Figure 2.

To assess the chemical stability of the scaffolds, ATR-FTIR was performed on the gels after 3 and 21 days. Representative ATR-FTIR spectra from day 3 were gathered and subtracted from day 21 spectra to elucidate the difference in vibrational peaks between both time points, as shown in Figure 3C. Peaks at 1588 and 1415 cm⁻¹ signify the symmetric and asymmetric stretching of -COO of carboxylic acids and are specific to ionic bonding. Peaks at 1078 cm⁻¹ relate to the C-C and C-O stretching. 18 The shoulder at 1078 cm⁻¹ is more prominent when alginate is cross-linked and when the relative ratio of gelatin in composite alginate-gelatin structures decreases. 18 The C-C stretching peak at 1021 cm⁻¹ had a reduced intensity after 21 days, signifying the onset of degradation of the alginate structure by loosening of cross-links from 15 days, as corroborated by swelling studies (Figure 2C). This degradation occurs in the "egg-box" structure of cross-linked alginate between guluronic acid residues as calcium ions are released. 19 Electrostatic repulsion between carboxylate anions enhances the swelling of alginate and eventually facilitates their release into the environment as soluble alginate molecules. 19 Based on our results, it may be inferred that the gelatin present in the structure may undergo sustained solubilization without affecting the mechanical stability and integrity of the scaffolds for the desired study period.

3.4. Rheological Analysis. The shear-thinning properties of hydrogel-based bioinks serve to reduce shear stress on encapsulated cells during 3D bioprinting, thereby increasing cell viability during the fabrication process. ^{14,20} Shear thinning also directly correlates to the structural fidelity of extrusion-

based bioinks.²⁰ Thus, to obtain high-resolution 3D bioprinted scaffolds, the shear-thinning characteristics of the alginate—gelatin bioink were studied through rheology and are represented in Supporting Figure S1. The viscosity of the bioink was observed to decrease with increasing shear rate, signifying the formulation observed shear-thinning behavior. During 3D printing, the increase of pressure in the nozzle decreased the viscosity of the hydrogel, thereby facilitating its deformation.¹⁴ Based on the obtained results, the consistency of the bioink was satisfactory for extrusion-based 3D bioprinting applications. All other compositions of the bioink that were used during the optimization process did not meet these criteria and/or did not retain structural integrity and robustness of the printed constructs for at least 21 days, which was a primary requirement for this study.

Rheometric analysis was performed on the 3D printed scaffolds after cross-linking (Supporting Figures S2 and S3), without swelling (day 0), and subjected to 3, 10, and 21 days of swelling (days 3-21). Amplitude and frequency sweeps were performed to determine if the strain and frequency range were within the linear viscoelastic (LVE) range of the gels. By examining the frequency dependence of the storage and loss moduli, important aspects such as the degree of cross-linking, entanglement, glass transition, and chain architecture of the gels can be inferred.²¹ At 10% constant strain, the non-crosslinked hydrogels behaved like a viscous liquid at lower frequencies and exhibited more elastic properties with increasing frequencies due to the decrease in relaxation time, which is attributed to the higher storage than loss modulus (data not included).²¹ After cross-linking with CaCl₂, the gels became steady, confirmed by the appearance of a plateau within the frequency sweep. Furthermore, the storage modulus on day 10 after swelling was seen to be significantly higher than the rest of the respective time points. On this day, hydrogels are seen to be in equilibrium swelling. The increase of outward pressure from absorbed media during this maximum swelling phase could be the main contributor to the observed increase in the elasticity of the scaffold. Rheological properties exhibited by the non-cross-linked gels were used as a control to confirm the cross-linking of the hydrogels. The structural stability and

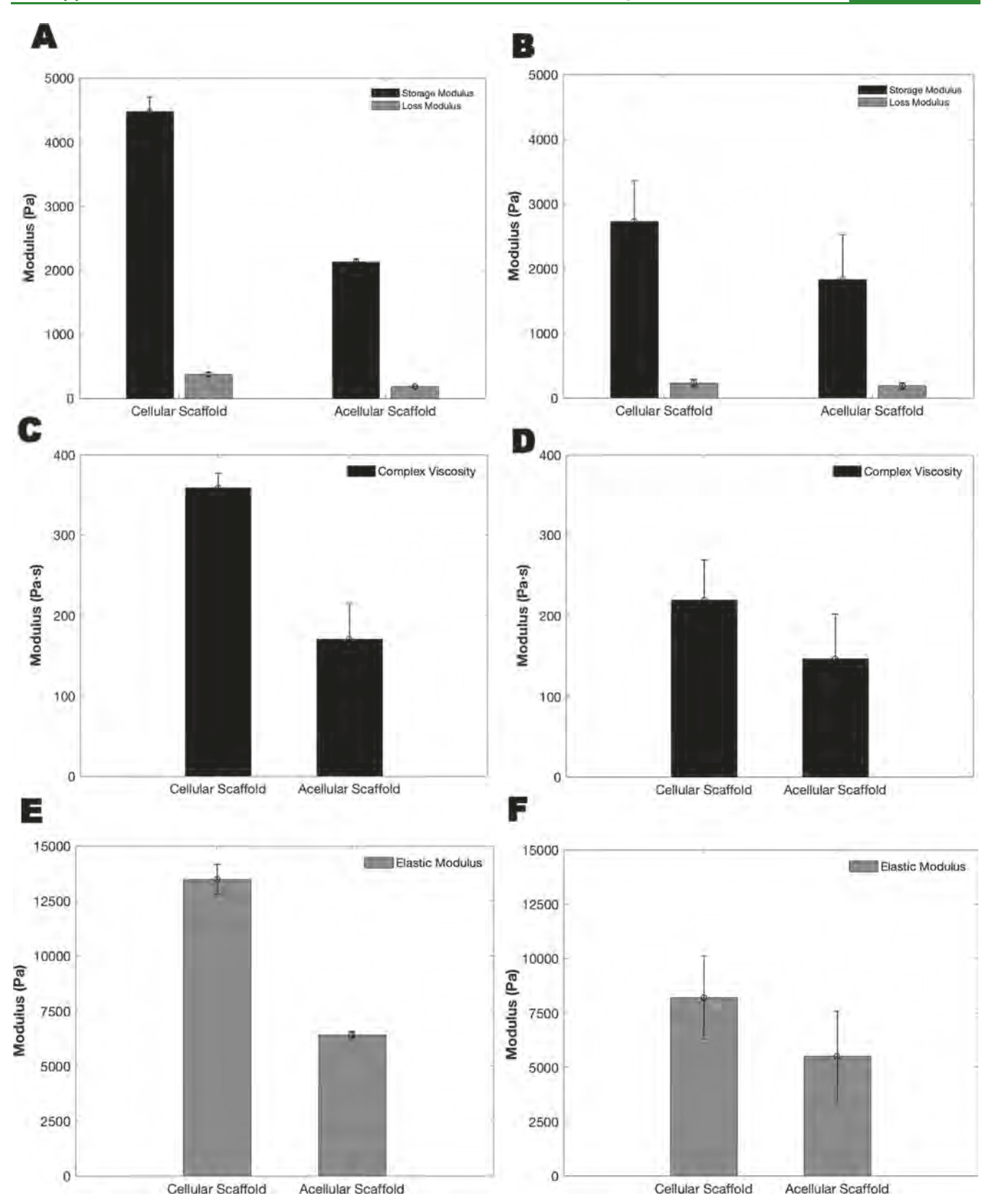


Figure 4. Rheometric analysis of 3D bioprinted cellular vs acellular scaffolds. Graphs (A, C, E) show the average storage/loss moduli, average complex viscosity, and average elastic modulus results, respectively, after 4 days of culture, where p-values were found to be statistically significant between the cellular and acellular scaffolds (p < 0.05). Graphs (B, D, F) show the average storage/loss moduli, average complex viscosity, and average elastic modulus results, respectively, after 11 days of culture, where p-values were not found to be statistically significant between the cellular and acellular scaffolds (p > 0.05).

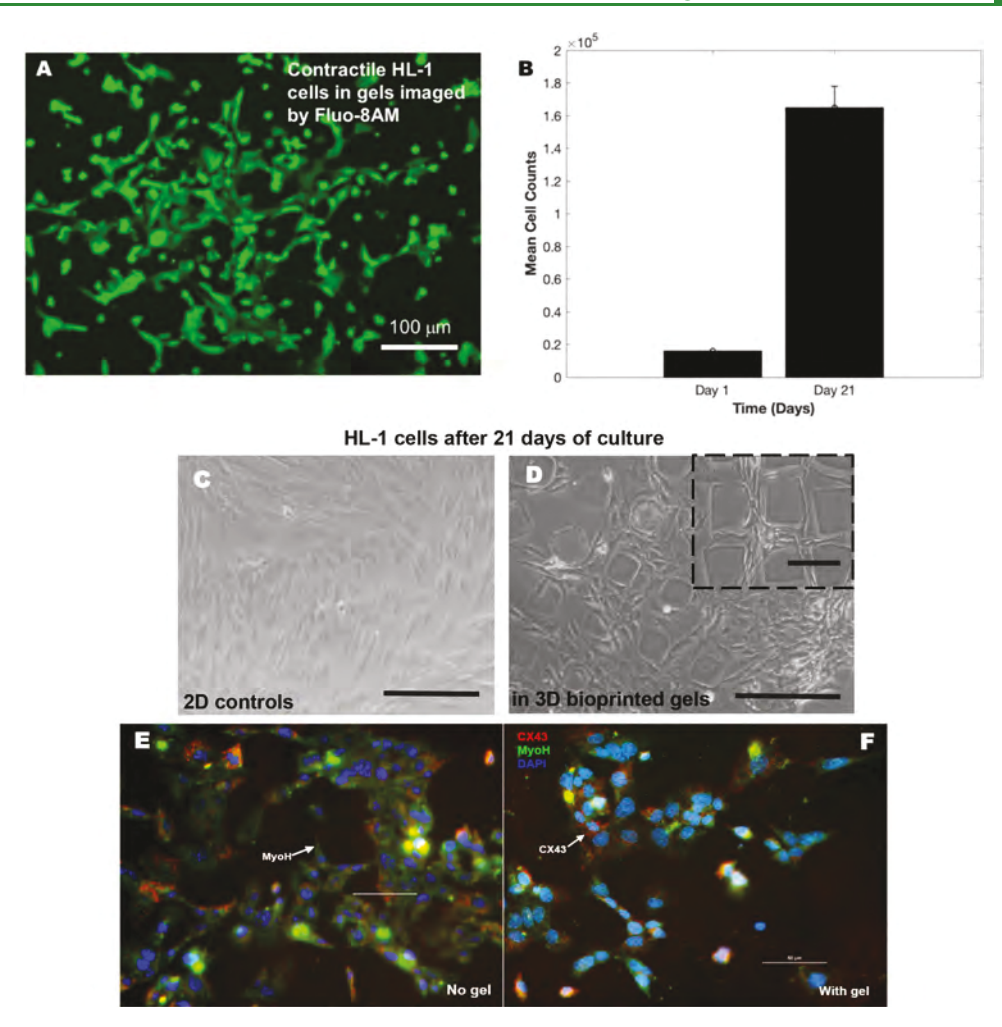


Figure 5. HL-1 contractile cardiomyocytes cultured within the 3D gels. (A) Image captured using the Fluo-8AM staining in the HL-1 cells in gels detecting their intracellular calcium mobilization. (B) Average cell densities isolated from cultures of HL-1 cells in gels on day 1 and after 21 days. (C, D) HL-1 cells cultured atop 2D controls and within gels up to 21 days are depicted in panels (C) and (D), respectively. Scale bar corresponds to 150 μ m in both images. (E, F) Immunohistochemistry of HL-1 contractile cardiomyocytes cultured within the gels (F) or on controls (E). The predominant cardiac markers including CX43 and MyoH expressions were confirmed for the HL-1 cells used in this study, while all cells were counterstained using the nuclear stain DAPI. Scale bar corresponds to 50 μ m in both images (E) and (F).

elasticity of the 3D printed hydrogels were found to increase after ionic cross-linking.

This study also evaluated the effect of encapsulating cells on the mechanical properties of the hydrogels during their in vitro incubation. Analysis was conducted on samples evaluated within the LVE range under a constant shear strain. Results presented in Figure 4A depict a significantly higher storage/ loss modulus in the cellular scaffolds (4476.9 \pm 228.3/369.56 \pm 27.5 Pa; p < 0.05) as compared to those in acellular scaffolds $(2127.4 \pm 54.6/182.01 \pm 5 \text{ Pa}; p < 0.05)$ on day 4. Likewise, the complex viscosity (4C) and elastic moduli (4E) appeared to be greater in the cellular scaffolds (359 \pm 18.1/13476.8 \pm 675.6 Pa; p < 0.05) with respect to those in acellular scaffolds $(171 \pm 43.4/6405.5 \pm 161.8 \text{ Pa}; p < 0.05)$ on day 4. All scaffolds degraded during in vitro incubation as shown by the reduction in the storage modulus on day 11 in both cellular and acellular scaffolds (Figure 4B). Yet, the cell-based scaffolds possessed an overall higher storage modulus compared to the acellular scaffolds, which confirmed that the incorporation of cells enhanced the mechanical properties of the 3D bioprinted hydrogels. Results in Figure 4B show that storage/loss modulus for the cell-encapsulated scaffolds was (2725.5 \pm

631/230.1 \pm 55.7 Pa; p > 0.05) in comparison to that for acellular scaffolds (1827.1 \pm 692.3/186.25 \pm 52.1 Pa; p > 0.05). Similarly, both the complex viscosity and the elastic moduli were higher in magnitude in the cellular scaffolds (219 \pm 50.6/8205.6 \pm 1900 Pa; p > 0.05) compared to those in the acellular scaffolds (147 \pm 55.5/5509.9 \pm 2081 Pa; p > 0.05), as depicted in Figure 4D,F respectively.

The extracellular matrix (ECM) is a complex and dynamic matrix that encircles cells in all tissues, providing mechanical and structural support while mediating numerous biological processes that are pivotal for supporting tissue formation and function. The observed increase of mechanical properties in the cellular scaffolds is consistent with the continuous production of the extracellular matrix by the encapsulated cells and the natural elongated and spindle-like shape mainly of cardiomyocytes and cardiac fibroblasts, the hydrogels and thus their mechanical properties. As a result, the results for cellular scaffold had a higher storage/loss modulus, complex viscosity, and elastic modulus than those for acellular scaffolds for each time point. However, we attributed the decrease in the mechanical properties between days 4 and

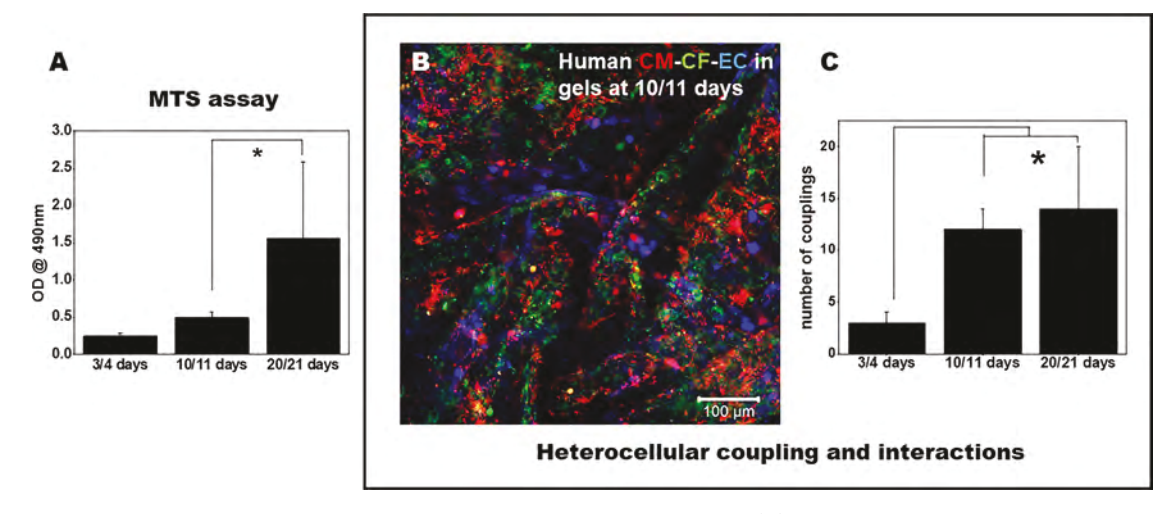


Figure 6. Viability of the cells and their heterocellular coupling in 3D printed scaffolds. (A) MTS assay of cells in 3D printed annular rings at various time points depicts cell viability and maintenance in long-term sustained cultures at 21 days. (B) Fluorescent microscopy image of CMs (red), CFs (green), and ECs (blue) in the 3D printed scaffolds (scale bar depicts $100 \mu m$). (C) Number of heterocellular couplings at various time points in this study.

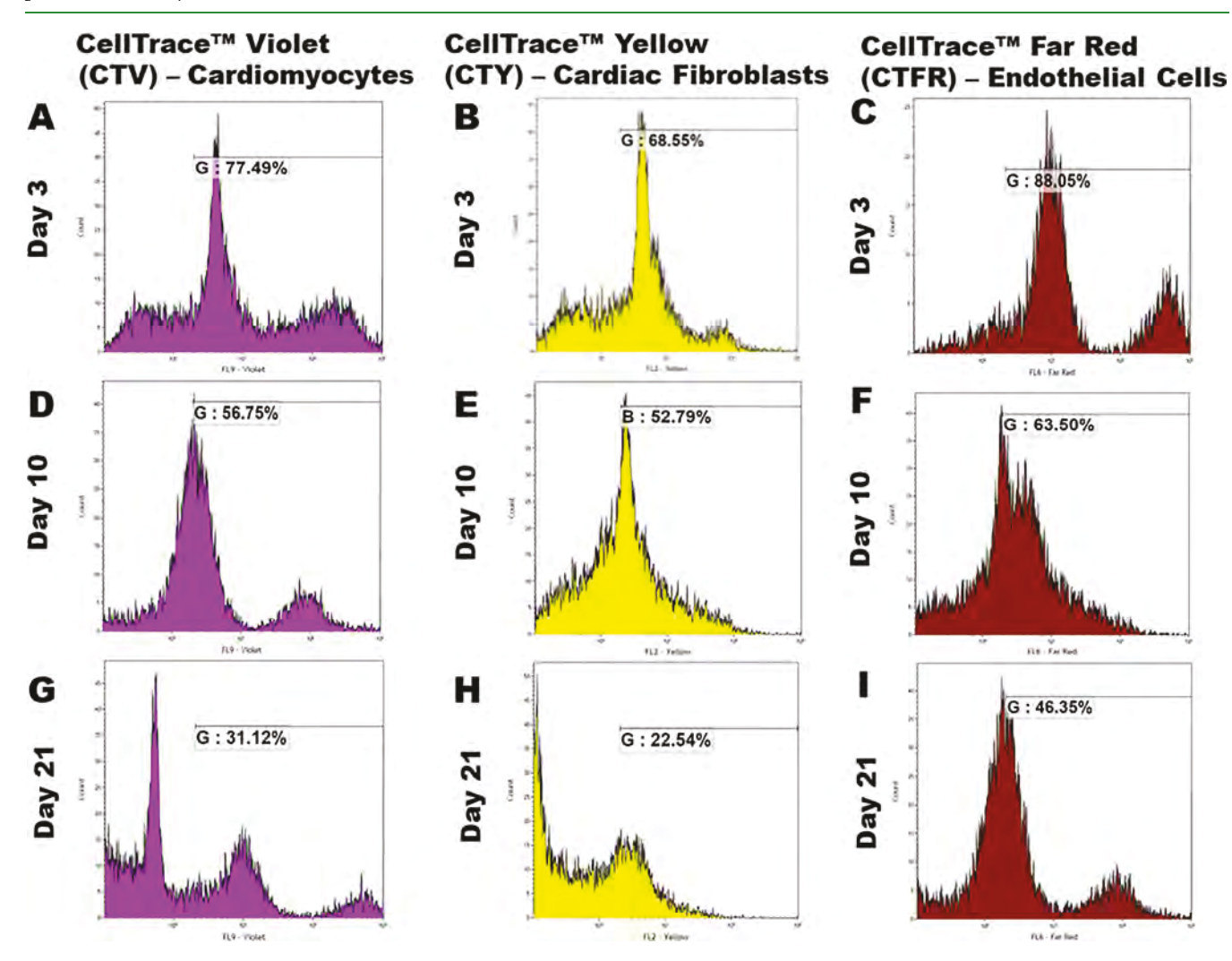


Figure 7. FACS analysis. Cardiomyocytes were stained with CellTrace Violet, cardiac fibroblasts with CellTrace Yellow, and endothelial cells with CellTrace Far Red and mixed in a 2:2:1 ratio with the bioink prior to 3D bioprinting. After 3, 10, and 21 days, cells were extracted from the scaffolds and analyzed using a flow cytometer. Graphs (A, D, G) show the % of CTV dye intensity, (B, E, H) show the % of CTY dye intensity, and (C, F, I) show the % of CTFR dye intensity for cardiomyocytes, cardiac fibroblasts, and endothelial cells, respectively. p-values were found to be all statistically significant between the different time points (p < 0.05).

Table 2. Percentage of Dye Intensity of Cardiomyocytes (CTV), Cardiac Fibroblasts (CTY), and Endothelial Cells (CTFR) in the 3D Bioprinted Scaffold on days 3, 10, and 21

dye color			
time point	celltrace violet (CTV) (%)	celltrace yellow (CTY) (%)	celltrace far red (CTFR) (%)
day 3	77.49	68.55	88.05
day 10	56.75	52.79	63.5
day 21	31.12	22.54	46.35

11 to the reduction of the cross-linking density between the neighboring polymer network creating deficiency and weakness among the alginate—gelatin polymers. ^{30,31} In addition, after 11 days of in vitro incubation, the biodegradation of all of the cellular scaffolds was confirmed probably due to the combined effects of the hydrogel's spontaneous degradation and hydrolysis with the enzymatic activity associated with the release of proteases such as metalloproteases as cells continuously proliferated. ^{30,31}

3.5. Cardiac Contractility. HL-1 cardiomyocytes were bioprinted within the hydrogel scaffolds to assess the effect on their contractile function. Figure 5A shows a representative image of Fluo-8AM stained contractile HL-1 cardiomyocyte cells in hydrogel scaffolds. The beating rate of the cells in scaffolds (38–42 bpm; see online Supporting Video File) did not vary significantly from the cells cultured on 2D controls. Online Supporting Videos showing the contraction depicted by the cells are also included. Results from our 21 day study showed increasing cell counts during the entire culture duration, confirming the biocompatibility of these scaffolds (Figure 5B). Figure 5C,D depicts bright-field images of HL-1 cells within 3D bioprinted scaffolds (5D) in comparison with 2D controls (5C), confirming the biocompatibility of these scaffolds toward long-term culture sustenance.

Figure 5E,F represents the immunohistochemical validation of the presence of the essential cardiac biomarkers CX43 and MyoH in the HL-1 cells in controls and in the 3D gels, respectively. This confirms the ability of the hydrogel scaffolds to support the viability and function of the HL-1 cardiomyocytes and cardiac cells in general to bioengineer the beating cardiac tissue.

3.6. Cell Viability and Proliferation within the Scaffolds. Figure 6A shows the absorbance of the soluble formazan dye generated by the viable cardiac cells (CMs, CFs, and ECs) at varying time points studied (3, 10, 21 days). A significant increase in the viability of cells confirmed by an enhanced absorbance of the formazan dye generated between 3 and 21 days represents the growth of the cells in the scaffolds. Since a significant increase in cell viability was noted in this study at increasing time points, the slow onset of degradation of the scaffolds allowed the cells to grow, thereby leading to an increase in their viability.

To study the proliferation behavior of the three cell types in the 3D bioprinted scaffolds, cells were extracted at each time point and analyzed using a flow cytometer over a 21 day study period. For this experiment, cardiomyocytes, cardiac fibroblasts, and endothelial cells were stained using CellTrace Violet (CTV), CellTrace Yellow (CTY), and CellTrace Far Red (CTFR) proliferation dyes and mixed with the bioink in a 2:2:1 ratio, respectively. Based on the concept of dye dilution, this allowed us to examine the proliferation of cells encapsulated in the 3D bioprinted scaffold, which, in turn, causes a reduction in the respective dye intensity over multiple generations. Supporting Figure 4 demonstrates character-

istic peaks of negative controls where none of the three cell types were stained and for positive controls in which each cell type was incubated with its respective dye, labeled alongside the figure. The cell extract after 3 days of culture showed the reduction in dye intensity for all three cell types as shown in Figure 7 when compared to their respective positive control values (maximum intensity). The average intensities of the dyes from extracted cells stained with CTV, CTY, and CTFR, respectively, reduced gradually from 77.49, 68.55, and 88.05% on day 3 to 56.75, 52.79, and 63.5% on day 10, as shown in Figure 7. After 21 days, the average dye intensities were recorded at 31.12, 22.54, and 46.35% on day 21 for cardiomyocytes, cardiac fibroblasts, and endothelial cells, respectively, as depicted in Figure 7. This significant decrease in dye intensity between the different time points (p < 0.05) clearly confirmed proliferation for the three cell types present in the scaffold (Table 2).

The reduction of dye intensity clearly suggested the dilution of the dyes with time indicating cell proliferation within the scaffold throughout the 21 day culture period. The maximum rate of reduction of dye intensity was shown in cardiac fibroblasts compared with those in cardiomyocytes and endothelial cells, which was consistent with the existing literature suggesting that cardiac fibroblasts multiply at a higher rate when compared to cardiomyocytes and endothelial cells. 34–36

3.7. Confirmation of Cardiac Heterocellular Interaction and Paracrine Signaling. We could identify and observe direct communication between all of the cells, CMs, CFs, and ECs, in the bioprinted scaffold, as seen in Figure 6B, after 10-11 days of culture. The extent of the number of cell couplings improved with time and was significantly greater at 10-11 days, which continued to increase, reaching a peak at 20-21 days, compared to earlier time points (Figure 6C). These results also corroborate and confirm the trends found in the MTS assay results. In this study, we confirmed the heterocellular coupling normally exhibited between CM and CF as also shown by our previous studies³ and by the expression of FSP-1 by the CF and CX43 by the CM, as depicted in Supporting Figure S4. Due to the introduction of a third cell type, we expected all of the cells to communicate with each other through direct cell-cell interactions (CM-CF) and paracrine signaling (between EC and other cells), as both homotypic and heterotypic cell interactions contribute to the organized structure and proper function of the heart.³ CMs are known to physically connect and communicate with CFs through gap junctions; however, they also seemed to communicate with ECs through both direct physical contacts and paracrine signaling, as seen in high-magnification image panels depicted in Figure 8 and Supporting Figure S5. In addition, the maintenance of cell phenotype and the interaction between all three cells (in gels) was consistently maintained throughout the entire study period (Figure 8 and Supporting Figures S5–S7).

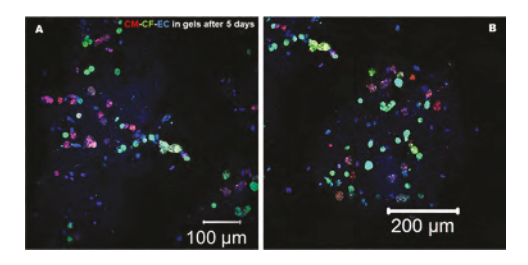


Figure 8. Immunohistochemistry was performed to probe the presence and the mechanism of interaction with other cells for the EC in bioprinted gels after 5 days of culture. CM and CF were prestained with PKH26 (red) and PKH67 (green), respectively. The ECs were immunostained using primary followed by secondary antibodies targeted toward CD31 (blue). The magnified figure insets are presented in Supporting Figures S5–S7.

4. DISCUSSION

Understanding the cellular and molecular mechanisms involved in the progression of cardiac diseases can help early identification of patients who are at high risk or in the initial stages of developing cardiac dysfunction.^{37,38} This will also lead to the identification of new therapeutic targets for the prevention and treatment of cardiac diseases. No wellestablished cardiac tissue platform currently exists that can be used as a basis for such studies although human pluripotent stem-cell-derived cardiomyocytes have been used with limited success to develop human heart-on-a-chip platforms in the past.³⁹ Establishment of a 3D cell model system is of prime importance to study the resultant effects on cardiac tissues under environmental stressors and conditions known to modulate the development of cardiac diseases. Current strategies to accomplish this goal include the differentiation of cardiac progenitor or induced pluripotent stem cells into mature and functional cardiac cells leading to the growth of functional cardiac tissues on biomaterial scaffolds that support the tissue's growth and development.³⁹ However, all such 3D cardiac tissue platforms have a limited longevity and lack robustness; so, our goal in this study was to biofabricate a robust human cardiac tissue platform using human cardiac cells that have sustained longevity and function.

Our key objective was to create a 3D cardiac tissue-mimicking model that may allow for a better understanding of cardiac biology and facilitate the study of cardiac biomarkers for a sustained period. We successfully achieved the high-throughput production of 3D scaffolds that are structurally and mechanically stable with highly interconnected pores that promoted long-term cell viability, function, and maintenance of cell phenotypes while engaging in heterocellular interactions.³ The extrusion printing process adopted for the biofabrication of cardiac tissues is not known to affect cellular viability in the long term, as depicted by prior published works from our laboratory.^{3,13} In addition, the alginate with high guluronic acid mixed with gelatin in the bioink presented an enhanced number of cell binding motifs, thereby enabling a higher cell viability and proliferation during the entire culture period.

In the cardiac wall, cardiac myocytes, fibroblasts, and endothelial cells form extensive networks in the heart, with direct and indirect communications between these cell types. In our previously published studies, we have demonstrated proof of *in vitro* heterocellular coupling between cardiomyocytes and cardiac fibroblasts via connexin-43 (Cx43) gap junction, facilitated by 3D bioprinting *in vitro*.³ This

heterocellular coupling phenomenon is key to understanding the potential active contribution of nonmyocytes to cardiac electrophysiology and their relevance toward cardiac structure and function. 40-42 Our results highlight the importance of direct cell-cell communication in the heart, as the interactions between CMs, CFs, and ECs result in differential cardiac cytokine expression, which has many implications for the process of cardiac remodeling and overall heart function during development and disease. Cardiomyocytes are known to produce and secrete cytokines for paracrine signaling with other cardiac cells and for endocrine signaling with peripheral tissues. Examples include natriuretic peptides A (ANP) and B (BNP), which act as cardioprotective factors mainly for CMs but also exert bidirectional effects on ECs. 42 On the other hand, the main cytokine, vascular endothelial growth factor (VEGF) secreted by the ECs, is known to protect the CMs and maintain cardiac physiology. We developed an organoid model for promoting the heterocellular coupling between cardiac myocytes and cardiac fibroblasts as well as promoting paracrine signaling from endothelial cells. Our model is versatile and can be adopted for the analysis of cell behavior and function in various other tissue engineering applications. 43-45 Others have used similar non-3D printed ring-like models to study arrhythmia and confirm its usefulness by applying relevant pharmacological interventions.⁴⁵

The addition of alginate with a high guluronic acid content is known to yield more stable structures that have been shown to retain excellent structural fidelity after 14 days of incubation in saline at 37 °C. 46 In this study, we demonstrated the longlasting structural robustness of the 3D bioprinted scaffolds up to 21 days using a waffle-like structure, which has the potential to resemble the striated framework of the actual in vivo cardiac tissue while maintaining peripheral accessibility of gas exchange and nutrients. Moreover, the structure is also expected to permit a low and homogeneous flow-induced shear stress on cells inside the scaffold.⁴⁵ In addition, the gelatin moiety in the bioink was not chemically cross-linked in this study, which can be cross-linked to enhance and sustain the biodegradability of the structure via replacement of gelatin with gelatin-methacrylate (GelMA) groups, which can be cross-linked using visible light exposure and a photoinitiator.⁴⁷

Although our study focused on recapitulating essential cardiac physiology using cardiomyocytes, cardiac fibroblasts, and cardiac endothelial cells, others have proposed mixtures of cardiomyocytes, cardiac-resident macrophages, pericytes, and fibroblasts to depict cellular homogeneity and define the complexity of the cardiac vasculature.⁴⁸ In future, we aim to work with microvessel fragments (MFs) isolated from adipose that are known to retain angiogenic potential *in vitro* and form a mature, perfused network when implanted. These MFs are rich in provascularizing cells that could uniquely drive neovascularization in 3D bioprinted constructs.⁴⁹

Our results highlight the cellular heterogeneity of the 3D bioprinted constructs in this study and reveal distinct cell-to-cell interactions among cardiomyocytes, cardiac fibroblasts, and cardiac endothelial cells. We successfully demonstrated the heterocellular interaction between these essential cardiac cells, and in future, our model can be expanded to accommodate more cardiac and noncardiac cell types for further studies. The tissue constructs that are developed in culture after 21 days depict complexity and maturity compared to earlier time points, therefore pointing toward the ability of these cardiac constructs to support tissue growth/development. Others have

shown similar effects of culturing cardiomyocytes induced from human-induced pluripotent stem cells (hiPSCs) alongside CFs and ECs. 50 These hiPSC-CMs are functionally immature, but on coculturing with CFs and EC, the CMs depicted improved maturity, leading to better sarcomeric structures compared with single-cultured CMs. 50

In this study, we investigated the overall cell proliferation trends in the 3D bioprinted constructs. Owing to the fact that all cells within the construct exhibit cellular networking, we did not intend to dissociate the clusters into single cells to study their proliferation and viability. The overall increase in cell viability matched well with the increase in heterocellular coupling in the entire construct, which implied that generally all cells survived and maintained viability and functionality in the construct via a sustained period. In parallel ongoing studies in our laboratory, we were specifically interested to study the proliferation trends for CM when they are coupled with the CF in 3D spheroidal droplets.³⁴ Results clearly showed that during the first 14 days of culture there was a steady peak indicating the proliferation of CM.³⁴ After 14 days of culture, the CM peaks were seen to be flattening out since they were being outnumbered by CFs, which grow more robustly and at a faster rate compared to CMs.³⁴ The ECs are expected to maintain a steady turnover when mixed with CMs and ECs.

In addition, to confirm the biocompatibility of the bioink as well as the entire extrusion printing process toward the retention of cardiac contractile function, we demonstrated contractile behavior via encapsulation of HL-1 cells in the 3D printed constructs. To the best of our knowledge, this is the first report of 3D bioprinting of HL-1 cells in gels confirming the retention of the autonomous beating of these cells in 3D gels. Others have either cultured HL-1 cardiomyocytes on top of the plated PEGylated fibrin (2D) or embedded in 3D gels that were manually made and concluded that a flat sheet-like construct is an absolute requirement for myocardial regeneration using HL-1 cells.⁵¹ However, we for the first time highlighted the role and benefit of 3D printing where cells are homogeneously mixed within gels, which facilitates their communication and networking eventually leading up to their contractile cardiac function.

While there have been numerous studies in space on the cardiac responses and genetic and epigenetic profiling on the effects of microgravity on the cardiac tissue, there is an unmet need for examining the underlying cellular mechanisms of the cardiovascular system that are activated due to microgravity exposure. Therefore, additional comparison between experiments on Earth and the International Space Station (ISS) needs to be performed to validate the simulations conducted on the ground and enable new research to simulate microgravity-based conditions, which will allow investigation into space mechanobiology with greater precision and control. Using original CubeLab technologies provided by Space Tango (Lexington, KY) to enhance microgravity-based research in the area of cardiac disease and development, the primary focus of this study was to integrate our 3D bioprinted cardiac tissue platform within the hardware provided by Space Tango for assessment of the effects of microgravity in cardiac disease development in a future study. In this study, we built a 3D bioprinted cardiac organoid system using three major cardiac cell types (CM, CF, and EC) as an in vitro model and tested its integration and functional validation via hardware implementation within the CubeLab. However, this system was only used to validate the cardiac tissue platform biofabricated inhouse under Earth's gravity. Future work will address the effect of microgravity on these 3D bioprinted cardiac organoids aboard the ISS.

The experimental design and layout in this study will provide desirable system conditions for installation of the 3D bioprinted cardiac tissues aboard the ISS, within Space Tango's research platform. The system is designed to conduct research in parallel with proving the system viability for sustained and long-term studies aboard the ISS that could utilize the system. The CubeLab system will be used to house, stabilize, and manage the experimental environment and data handling. The research platform aboard the ISS will provide power and data communications between Earth and the ISS.

5. CONCLUSIONS

In this study, a 3D bioprinted cardiac tissue model was developed using cardiac cells mixed in gelatin and alginate with high guluronic acid for a better understanding of cardiac biology and the study of cardiac biomarkers. The 3D scaffolds were structurally and mechanically stable with highly interconnected pores that promoted long-term cell viability, function, and maintenance of cell phenotypes over a sustained cultured period. The model also promoted heterocellular coupling between cardiac myocytes and cardiac fibroblasts in addition to engaging the endothelial cells via paracrine signaling. The 3D model is versatile and can be a potential tool for analyzing cell behavior and function in various other applications such as drug screening and tissue engineering. To improve the mechanical and structural stability of the scaffolds, gelatin may be cross-linked, and a circular waffle design can be adopted for mimicking the anisotropic structure of in vivo cardiac tissue. Moreover, MFs rich in provascularizing cells may be used to replace endothelial cells to drive neovascularization in vitro leading to the formation of matured and perfused vessel networks within 3D bioprinted constructs that are more adoptable to testing under dynamic culture conditions.

ASSOCIATED CONTENT

Solution Supporting Information

The Supporting Information is available free of charge at https://pubs.acs.org/doi/10.1021/acsami.1c23883.

Bioink optimization, detailed rheological characterization of the bioink (Figures S1–S7) (PDF) Supporting video of beating Hl-1 cells in gels (MP4)

AUTHOR INFORMATION

Corresponding Author

Binata Joddar – Inspired Materials & Stem-Cell Based Tissue Engineering Laboratory (IMSTEL), The University of Texas at El Paso, El Paso, Texas 79968, United States; Department of Metallurgical, Materials, and Biomedical Engineering, M201 Engineering and Border Biomedical Research Center, The University of Texas at El Paso, El Paso, Texas 79968, *United States;* © orcid.org/0000-0002-9157-3140; Phone: +1(915)747-8456; Email: bjoddar@utep.edu; Fax: +1(915)747-8036

Authors

Matthew Alonzo - Inspired Materials & Stem-Cell Based Tissue Engineering Laboratory (IMSTEL), The University of Texas at El Paso, El Paso, Texas 79968, United States;

- Department of Metallurgical, Materials, and Biomedical Engineering, M201 Engineering, The University of Texas at El Paso, El Paso, Texas 79968, United States
- Raven El Khoury Inspired Materials & Stem-Cell Based Tissue Engineering Laboratory (IMSTEL), The University of Texas at El Paso, El Paso, Texas 79968, United States; Department of Metallurgical, Materials, and Biomedical Engineering, M201 Engineering, The University of Texas at El Paso, El Paso, Texas 79968, United States
- Naveen Nagiah Inspired Materials & Stem-Cell Based Tissue Engineering Laboratory (IMSTEL), The University of Texas at El Paso, El Paso, Texas 79968, United States; Department of Metallurgical, Materials, and Biomedical Engineering, M201 Engineering, The University of Texas at El Paso, El Paso, Texas 79968, United States
- Vikram Thakur Department of Molecular and Translational Medicine, Center of Emphasis in Diabetes and Metabolism, Texas Tech University Health Sciences Center, El Paso, Texas 79905, United States
- Munmun Chattopadhyay Department of Molecular and Translational Medicine, Center of Emphasis in Diabetes and Metabolism, Texas Tech University Health Sciences Center, El Paso, Texas 79905, United States

Complete contact information is available at: https://pubs.acs.org/10.1021/acsami.1c23883

Author Contributions

¹M.A. and R.E.K. contributed equally to this work. B.J. and M.C. conceived the study for this manuscript. The manuscript was written through contributions of all authors based on their respective participation. M.A., R.E.K., and N.N. performed all experiments under the guidance, mentoring, and supervision of B.J., V.T., and M.C. helped with the HL-1 experiments, the heterocellular coupling of CM–CF and EC along with relevant data analysis for the manuscript. All authors have given approval to the final version of the manuscript, and the authors declare no competing financial interest.

Notes

The authors declare no competing financial interest.

ACKNOWLEDGMENTS

This study was funded by the NSF grant, ISS/Collaborative Research: Studying the Effects of Microgravity on 3D Cardiac Organoid Cultures to Dr. Joddar and Dr. Chattopadhyay. The Joddar laboratory (IMSTEL) acknowledges NSF grant/s # 1828268 and # 1927628 and NIH SC1 grant #1SC1HL154511-01. MA acknowledges the Gates Millenium Fellowship and the Eloise and Patrick Wieland Graduate Fellows Program at UTEP. The Chattopadhyay lab acknowledges NSF grant # 1949909. The authors acknowledge the technical assistance received from Armando Varela (for confocal microscopy and FACS analysis), Michael Lyubchenko (for SEM), Carla Loyola (for biological experimental support), Joe A. Mudloff (for 3D bioprinting), Diego Bermudez (for ATR-FTIR), and Salma Ramirez (for CAD drawing). Blanca P. Ortega's help is gratefully acknowledged for English editing services for this manuscript.

REFERENCES

(1) Alonzo, M.; AnilKumar, S.; Roman, B.; Tasnim, N.; Joddar, B. 3D Bioprinting of cardiac tissue and cardiac stem cell therapy. *Transl. Res.* 2019, 211, 64–83.

- (2) Alonzo, M.; Kumar, S. A.; Allen, S.; Delgado, M.; Alvarez-Primo, F.; Suggs, L.; Joddar, B. Hydrogel scaffolds with elasticity-mimicking embryonic substrates promote cardiac cellular network formation. *Prog. Biomater.* **2020**, *9*, 125–137.
- (3) Anil Kumar, S.; Alonzo, M.; Allen, S. C.; Abelseth, L.; Thakur, V.; Akimoto, J.; Ito, Y.; Willerth, S. M.; Suggs, L.; Chattopadhyay, M.; Joddar, B. A Visible Light-Cross-Linkable, Fibrin-Gelatin-Based Bioprinted Construct with Human Cardiomyocytes and Fibroblasts. ACS Biomater. Sci. Eng. 2019, 5, 4551–4563.
- (4) Murphy, S. V.; Atala, A. 3D bioprinting of tissues and organs. *Nat. Biotechnol.* **2014**, *32*, 773–785.
- (5) Srikanth, G.; Prakash, P.; Tripathy, N.; Dikshit, M.; Nityanand, S. Establishment of a rat model of myocardial infarction with a high survival rate: A suitable model for evaluation of efficacy of stem cell therapy. *J. Stem Cells Regen. Med.* **2009**, *5*, 30–36.
- (6) Maiullari, F.; Costantini, M.; Milan, M.; Pace, V.; Chirivi, M.; Maiullari, S.; Rainer, A.; Baci, D.; Marei, H. E.; Seliktar, D.; Gargioli, C.; Bearzi, C.; Rizzi, R. A multi-cellular 3D bioprinting approach for vascularized heart tissue engineering based on HUVECs and iPSC-derived cardiomyocytes. *Sci. Rep.* **2018**, *8*, No. 13532.
- (7) Owen, T. J.; Harding, S. E. Multi-cellularity in cardiac tissue engineering, how close are we to native heart tissue? *J. Muscle Res. Cell Motil.* **2019**, *40*, 151–157.
- (8) Enobakhare, B.; Bader, D. L.; Lee, D. A. Concentration and M/G ratio influence the physiochemical and mechanical properties of alginate constructs for tissue engineering. *J. Appl. Biomater. Biomech.* **2006**, *4*, 87–96.
- (9) Su, K.; Wang, C. Recent advances in the use of gelatin in biomedical research. *Biotechnol. Lett.* **2015**, 37, 2139–2145.
- (10) Zhang, H.; Cheng, J.; Ao, Q. Preparation of alginate-based biomaterials and their applications in biomedicine. *Mar. Drugs* **2021**, 19, 264
- (11) Maity, C.; Das, N. Alginate-Based Smart Materials and Their Application: Recent Advances and Perspectives. *Top. Curr. Chem.* **2022**, 380, No. 3.
- (12) Claycomb, W. C.; Lanson, N. A., Jr.; Stallworth, B. S.; Egeland, D. B.; Delcarpio, J. B.; Bahinski, A.; Izzo, N. J., Jr. HL-1 cells: a cardiac muscle cell line that contracts and retains phenotypic characteristics of the adult cardiomyocyte. *Proc. Natl. Acad. Sci. U.S.A.* **1998**, 95, 2979—2984.
- (13) AnilKumar, S.; Allen, S. C.; Tasnim, N.; Akter, T.; Park, S.; Kumar, A.; Chattopadhyay, M.; Ito, Y.; Suggs, L. J.; Joddar, B. The applicability of furfuryl-gelatin as a novel bioink for tissue engineering applications. *J. Biomed. Mater. Res., Part B* **2019**, *107*, 314–323.
- (14) Zhang, X.; Zhang, Y. Tissue Engineering Applications of Three-Dimensional Bioprinting. *Cell Biochem Biophys* **2015**, *72*, 777–782.
- (15) Zhou, P.; Pu, W. T. Recounting Cardiac Cellular Composition. *Circ. Res.* **2016**, *118*, 368–370.
- (16) Phillips, S. N. Development of Cubelab for Plant Microgravity Research. MSc Thesis, 2016 (https://scholarworks.moreheadstate.edu/cgi/viewcontent.cgi?).
- (17) Sharma, A.; Puri, V.; Kumar, P.; Singh, I. Rifampicin-loaded alginate-gelatin fibers incorporated within transdermal films as a fiber-in-film system for wound healing applications. *Membranes* **2021**, *11*, 7.
- (18) Ma, X. Y.; Ding, C.; Li, H.; Jiang, K.; Duan, S.; Cai, W. B. Revisiting the Acetaldehyde Oxidation Reaction on a Pt Electrode by High-Sensitivity and Wide-Frequency Infrared Spectroscopy. *J. Phys. Chem. Lett.* **2020**, *11*, 8727–8734.
- (19) Simpson, N. E.; Stabler, C. L.; Simpson, C. P.; Sambanis, A.; Constantinidis, I. The role of the CaCl2–guluronic acid interaction on alginate encapsulated β TC3 cells. *Biomaterials* **2004**, *25*, 2603–2610.
- (20) Zhang, Y. S.; Khademhosseini, A. Advances in engineering hydrogels. *Science* **2017**, *356*, No. eaaf3627.
- (21) Stowers, R. S.; Allen, S. C.; Suggs, L. J. Dynamic phototuning of 3D hydrogel stiffness. *Proc. Natl. Acad. Sci.* **2015**, *112*, 1953–1958.
- (22) Theocharis, A. D.; Manou, D.; Karamanos, N. K. The extracellular matrix as a multitasking player in disease. *FEBS J.* **2019**, 286, 2830–2869.

- (23) Tonti, O. R.; Larson, H.; Lipp, S. N.; Luetkemeyer, C. M.; Makam, M.; Vargas, D.; Wilcox, S. M.; Calve, S. Tissue-specific parameters for the design of ECM-mimetic biomaterials. *Acta Biomater.* **2021**, *132*, 83–102.
- (24) Piperigkou, Z.; Götte, M.; Theocharis, A. D.; Karamanos, N. K. Insights into the key roles of epigenetics in matrix macromolecules-associated wound healing. *Adv. Drug Delivery Rev.* **2018**, *129*, 16–36.
- (25) Garate-Carrillo, A.; Ramirez, I. Embryonary mouse cardiac fibroblast isolation. In *Mouse Embryogenesis*; Springer, 2018; pp 71–79.
- (26) Siamwala, J. H.; Pagano, F. S.; Dubielecka, P. M.; Zhao, A.; Chen, S.; Granston, H.; Rounds, S.; Gilbert, R. J. Identification of Human CD4+ Sub-population of Resident Cardiac Fibroblasts Linked to Inflammation-Mediated Cardiac Fibrosis. *bioRxiv* **2021**, No. 433023
- (27) Hussey, G. S.; Dziki, J. L.; Badylak, S. F. Extracellular matrix-based materials for regenerative medicine. *Nature Reviews Materials* **2018**, *3*, 159–173.
- (28) Nazari, H.; Kehtari, M.; Rad, I.; Ashtari, B.; Joghataei, M. T. Electrical stimulation induces differentiation of human cardiospherederived cells (hCDCs) to committed cardiomyocyte. *Mol. Cell. Biochem.* **2020**, 470, 29–39.
- (29) Paolillo, M.; Schinelli, S. Extracellular Matrix Alterations in Metastatic Processes. *International Journal of Molecular Sciences* **2019**, 20, 4947.
- (30) Sanderson, R. D.; Bandari, S. K.; Vlodavsky, I. Proteases and glycosidases on the surface of exosomes: Newly discovered mechanisms for extracellular remodeling. *Matrix Biol.* **2019**, 75-76, 160–169
- (31) Song, Y. Y.; Zhang, Y.; Ren, H. N.; Sun, G. G.; Qi, X.; Yang, F.; Jiang, P.; Zhang, X.; Cui, J.; Wang, Z. Q. Characterization of a serine protease inhibitor from Trichinella spiralis and its participation in larval invasion of host's intestinal epithelial cells. *Parasites Vectors* **2018**, *11*, No. 499.
- (32) Tario, J. D.; Conway, A. N.; Muirhead, K. A.; Wallace, P. K. Monitoring cell proliferation by dye dilution: considerations for probe selection. In *Flow Cytometry Protocols*, Springer, 2018; pp 249–299.
- (33) Horton, M. B.; Prevedello, G.; Marchingo, J. M.; Zhou, J. H.; Duffy, K. R.; Heinzel, S.; Hodgkin, P. D. Multiplexed division tracking dyes for proliferation-based clonal lineage tracing. *J. Immunol.* **2018**, 201, 1097–1103.
- (34) El Khoury, R.; Nagiah, N.; Delgado, M.; Mudloff, J. A.; Thakur, V.; Chattopadhyay, M.; Joddar, B. 3D Bioprinted Spheroidal Droplets for Engineering the Heterocellular Coupling between Cardiomyocytes and Cardiac Fibroblasts. *Cyborg and Bionic Systems* **2021**, 2021, No. 9864212.
- (35) Radisic, M.; Park, H.; Martens, T. P.; Salazar-Lazaro, J. E.; Geng, W.; Wang, Y.; Langer, R.; Freed, L. E.; Vunjak-Novakovic, G. Pre-treatment of synthetic elastomeric scaffolds by cardiac fibroblasts improves engineered heart tissue. *J. Biomed. Mater. Res. A* **2008**, *86A*, 713–724.
- (36) Lang, J. K.; Young, R. F.; Ashraf, H.; Canty, J. M., Jr. Inhibiting Extracellular Vesicle Release from Human Cardiosphere Derived Cells with Lentiviral Knockdown of nSMase2 Differentially Effects Proliferation and Apoptosis in Cardiomyocytes, Fibroblasts and Endothelial Cells In Vitro. *PLoS One* **2016**, *11*, No. e0165926.
- (37) Eagle, K. A.; Ginsburg, G. S.; Musunuru, K.; Aird, W. C.; Balaban, R. S.; Bennett, S. K.; Blumenthal, R. S.; Coughlin, S. R.; Davidson, K. W.; Frohlich, E. D.; Greenland, P.; Jarvik, G. P.; Libby, P.; Pepine, C. J.; Ruskin, J. N.; Stillman, A. E.; Van Eyk, J. E.; Tolunay, H. E.; McDonald, C. L.; Smith, S. C., Jr. Identifying patients at high risk of a cardiovascular event in the near future: current status and future directions: report of a national heart, lung, and blood institute working group. *Circulation* **2010**, *121*, 1447–1454.
- (38) Lee, R. T.; Walsh, K. The Future of Cardiovascular Regenerative Medicine. *Circulation* **2016**, *133*, 2618–2625.
- (39) Suh, T. C.; Amanah, A. Y.; Gluck, J. M. Electrospun Scaffolds and Induced Pluripotent Stem Cell-Derived Cardiomyocytes for

- Cardiac Tissue Engineering Applications. *Bioengineering* **2020**, *7*, No. 105.
- (40) Kohl, P.; Gourdie, R. G. Fibroblast-myocyte electrotonic coupling: does it occur in native cardiac tissue? *J. Mol. Cell. Cardiol.* **2014**, 70, 37–46.
- (41) Lo, C. W.; Wessels, A. Cx43 gap junctions in cardiac development. *Trends Cardiovasc. Med.* **1998**, *8*, 264–269.
- (42) Talman, V.; Kivela, R. Cardiomyocyte-Endothelial Cell Interactions in Cardiac Remodeling and Regeneration. *Front. Cardiovasc. Med.* **2018**, 5, No. 101.
- (43) Chaulin, A. M.; Abashina, O. E.; Duplyakov, D. V. Pathophysiological mechanisms of cardiotoxicity in chemotherapeutic agents. *Russ. Open Med. J.* **2020**, *9*, No. e0305.
- (44) Polonchuk, L.; Chabria, M.; Badi, L.; Hoflack, J.-C.; Figtree, G.; Davies, M. J.; Gentile, C. Cardiac spheroids as promising in vitro models to study the human heart microenvironment. *Sci. Rep.* **2017**, *7*, No. 7005.
- (45) Goldfracht, I.; Protze, S.; Shiti, A.; Setter, N.; Gruber, A.; Shaheen, N.; Nartiss, Y.; Keller, G.; Gepstein, L. Generating ringshaped engineered heart tissues from ventricular and atrial human pluripotent stem cell-derived cardiomyocytes. *Nat. Commun.* **2020**, *11*, No. 75.
- (46) Darrabie, M. D.; Kendall, W. F.; Opara, E. C. Effect of alginate composition and gelling cation on microbead swelling. *J. Microencapsulation* **2006**, 23, 613–621.
- (47) Xiao, S.; Zhao, T.; Wang, J.; Wang, C.; Du, J.; Ying, L.; Lin, J.; Zhang, C.; Hu, W.; Wang, L.; Xu, K. 2019. Gelatin methacrylate (GelMA)-based hydrogels for cell transplantation: an effective strategy for tissue engineering. Stem Cell Rev. Rep. 2019, 15, 664–679.
- (48) Litviňuková, M.; Talavera-Lopez, C.; Maatz, H.; Reichart, D.; Worth, C. L.; Lindberg, E. L.; Kanda, M.; Polanski, K.; Heinig, M.; Lee, M.; Nadelmann, E. R.; Roberts, K.; Tuck, L.; Fasouli, E. S.; DeLaughter, D. M.; McDonough, B.; Wakimoto, H.; Gorham, J. M.; Samari, S.; Mahbubani, K. T.; Saeb-Parsy, K.; Patone, G.; Boyle, J. J.; Zhang, H.; Zhang, H.; Viveiros, A.; Oudit, G. Y.; Bayraktar, O. A.; Seidman, J. G.; Seidman, C. E.; Noseda, M.; Hubner, N.; Teichmann, S. A. Cells of the adult human heart. *Nature* 2020, 588, 466–472.
- (49) Nunes, S. S.; Krishnan, L.; Gerard, C. S.; Dale, J. R.; Maddie, M. A.; Benton, R. L.; Hoying, J. B. Angiogenic potential of microvessel fragments is independent of the tissue of origin and can be influenced by the cellular composition of the implants. *Microcirculation* **2010**, *17*, 557–567.
- (50) Giacomelli, E.; Meraviglia, V.; Campostrini, G.; Cochrane, A.; Cao, X.; Van Helden, R. W.; Garcia, A. K.; Mircea, M.; Kostidis, S.; Davis, R. P.; Van Meer, B. J.; et al. Human-iPSC-derived cardiac stromal cells enhance maturation in 3D cardiac microtissues and reveal non-cardiomyocyte contributions to heart disease. *Cell Stem Cell* **2020**, *26*, 862–879.
- (51) Geuss, L. R.; Allen, A. C.; Ramamoorthy, D.; Suggs, L. J. Maintenance of HL-1 cardiomyocyte functional activity in PEGylated fibrin gels. *Biotechnol. Bioeng.* **2015**, *112*, 1446–1456.